PERGAMON

Planetary and Space Science 50 (2002) 527–534

Planetary and Space Science

www.elsevier.com/locate/pss

On the magnetosheath thicknesses of interplanetary coronal mass ejections

C.T. Russell *, T. Mulligan

Department of Earth and Space Sciences, Institute of Geophysics and Planetary Physics, University of California Los Angeles, 3845 Slichter Hall, MS 156704, Los Angeles, CA 90095-1567, USA

Abstract

Interplanetary coronal mass ejections (ICMEs) often move relative to the ambient solar wind plasma at a speed that exceeds the fast magnetosonic velocity, producing a standing shock wave in the frame of the ICME and a magnetosheath whose plasma flows around the obstacle much as the terrestrial magnetosheath flows around the Earth's magnetosphere. The half-thickness of an ICME is typically 0.1 AU at 1 AU. If this dimension represented the characteristic scale size of the obstacle, then the thickness of the magnetosheath should be about 0.025 AU but it is typically closer to 0.1 AU. In order to treat this problem we convert the original Spreiter et al. (Planet. Space Sci. 14 (1966) 223) formula for the terrestrial magnetosheath thickness to one that is appropriate for the ICME magnetosheath. This treatment allows us to conclude that the characteristic radius of curvature of an ICME at 1 AU is about 0.4 AU. This radius of curvature is provided by both the bend of the axis of the rope and by an elongation of the ICME in the direction perpendicular to both the rope axis and the solar wind flow. Thus near 1 AU ICMEs have a radial thickness that is smaller than their other two characteristic dimensions.

1. Introduction

An interplanetary coronal mass ejection (ICME) is the disturbance seen in the solar wind resulting from a coronal mass ejection (CME). This disturbance often takes the form of a large enhancement of the magnetic field strength lasting a fraction of a day preceded by an interplanetary shock as the ICME moves rapidly through the ambient solar wind. Although identification of every ICME with a CME has not been made, sufficient identifications of the causative CME have been made for both the preceding shocks (Schwenn, 1983; Sheeley et al., 1985) and the following magnetic structure (Burlaga et al., 1982; Richardson et al., 1994; Lindsay et al., 1999) that we can have much confidence in the correctness of the association. There is some debate on what to call these magnetic structures and their associated plasma variations (Burlaga, 2001; Russell, 2001). Often these structures have a very regular magnetic pattern that has been termed a magnetic cloud (Burlaga et al., 1981). These regular structures have been interpreted as force-free magnetic flux ropes by Goldstein (1983) in which the outward magnetic field pressure of the rope is balanced by the inward curvature force of the bent magnetic field. This interpretation is similar to that of the magnetic structures found in the Venus ionosphere by Russell and Elphic (1979) but on a far smaller scale. The Venus ropes had radii measured in kilometers; the interplanetary flux ropes were of the order of 50 million km across.

It is very difficult to infer the true spatial structure of an interplanetary CME from observations along a single trajectory through the ICME. When the structure is smoothly varying such as in the structures Burlaga et al. (1981) have termed magnetic clouds, progress can be made by assuming that the clouds are cylindrically symmetric ropes and the structure determined by inversion procedures, assuming a force-free rope (Burlaga, 1988). This procedure has been applied to a large number of such structures (Lepping et al., 1990). The success of this approach has led to the paradigm of the ICME, and especially its subclass, magnetic clouds, as being rope-like structures with legs extending back to the sun. The frequent presence of bi-directional streaming electrons is consistent with either a model in which the rope field lines close on themselves or that both legs of the rope are connected to the sun. The observation of rapid

* Corresponding author. Tel.: +1-310-825-3188; fax: +1-310-206-3051.
E-mail address: ctrussel@igpp.ucla.edu (C.T. Russell).

0032-0633/02/$ - see front matter © 2002 Elsevier Science Ltd. All rights reserved.
PII: S0032-0633(02)00031-4

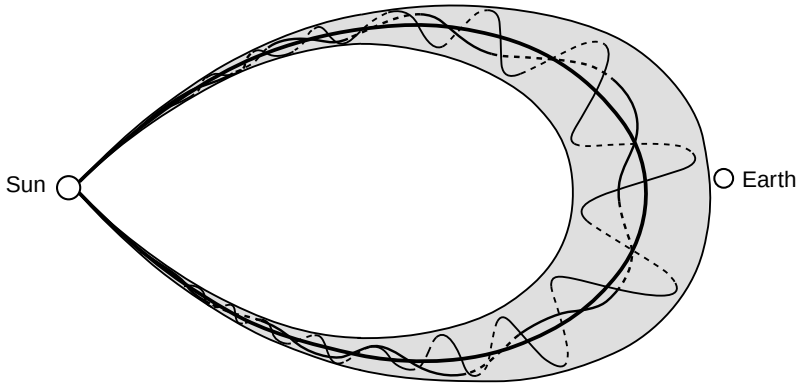

Fig. 1. The current paradigm of a simple ICME or magnetic cloud in which a twisted flux rope connects back to the solar corona. This model is based on a sketch by Burlaga et al. (1990) but modified according to the conclusions of Kahler and Reames (1991) to show connection to the surface of the sun.

transients in the bi-directional electrons in the ropes can determine which of these two possibilities is correct (Kahler and Reames, 1991). Farrugia et al. (1993a, b) applied this test and showed that indeed the field lines are connected to the sun and we have so modified the original sketch of Burlaga et al. (1990) in Fig. 1 to reflect the present understanding of the interconnection of these flux ropes to the sun.

While we cannot do better than this picture with single spacecraft measurements, the occasional multiple spacecraft observations and inferences based on statistical properties suggest that the paradigm shown in Fig. 1 needs modification. One such statistical constraint is the standoff distance of the bow shock that appears to be larger than predicted by the cylindrically symmetric flux-rope paradigm. In order to properly treat this problem we must transform earlier work on the standoff distance of the terrestrial bow shock, i.e. the thickness of the magnetosheath, into a form that can be applied to the ICME problem.

Although it is standard, in discussing the standoff distance of the terrestrial bow shock, to express it in terms of the distance of the nose of the obstacle to the center of the Earth, physically it is the radius of curvature of the nose of the obstacle that controls this standoff distance. Thus, our first task is to re-express Spreiter et al.'s (1966) formula for the standoff distance in terms of the radius of curvature of the obstacle. Then, because the Spreiter et al. formula is applicable to only high Mach number shocks, we rewrite the formulas in a form suitable for low Mach number shocks using the conjecture of Farris and Russell (1994).

One complication is that it is possible that an ICME has two characteristic radii of curvature, one pertaining to the axial bending of the rope and one pertaining to azimuthal stretching of the ICME perpendicular to the plane containing the axis of the rope. Stahara et al. (1989) treated this problem in order to explain the standoff distance of the jovian shock in front of the jovian magnetodisk that also has two radii of curvature.

We proceed in this study as follows. First, we examine some typical examples of ICMEs as observed by Wind and Near Earth Asteroid Rendezvous (NEAR) and the statistics of magnetosheath thicknesses seen by Pioneer Venus Orbiter (PVO). Then we develop the formulas for the standoff distance and apply them to the observations. Finally, we compare these inferences with those from other techniques.

2. Observations

Even from the magnetic field profile alone it is relatively simple to deduce the size of the ICME obstacle and its associated magnetosheath. Fig. 2 shows an example of an ICME (the so-called Bastille Day event) seen at 1 AU by the Advanced Composition Explorer (ACE) magnetometer (C.W. Smith personal communication, 2000). The leading shock is obvious at about 1415 UT and the inner edge of the magnetosheath is evident at about 1800 UT on July 15, 2000. As shown in Fig. 3, when the ICME reaches 1.7 AU, the shock stands off further from the obstacle so that the magnetosheath extends from about 1500 UT to 2400 UT on July 16 and the obstacle is correspondingly bigger. We emphasize that the ICME is expanding as it passes both observation points and that part of the profile observed is due to intrinsic temporal variation and not just the convection of a spatial profile by the spacecraft. The dashed lines on Figs. 2 and 3 show fits to the magnetic structure of the rope. The radius of the ICME inferred from a cylindrically symmetric fit in 0.25 AU at 1.0 AU and 0.43 AU at 1.7 AU. Thus the radius of the rope, or more correctly its thickness, has expanded in direct proportion to its radial distance. If the rope were cylindrically symmetric, as assumed, it would maintain the same angular width as it moves away from the sun. However, one possible problem is that this structure is only 14° across, whereas at the sun on the limbs CMEs generally subtend about 45°.

The orientations of the axis of the rope in these two fits are similar: cone angles of 92° and 76° at ACE and NEAR respectively (where 90° is perpendicular to the radial direc-

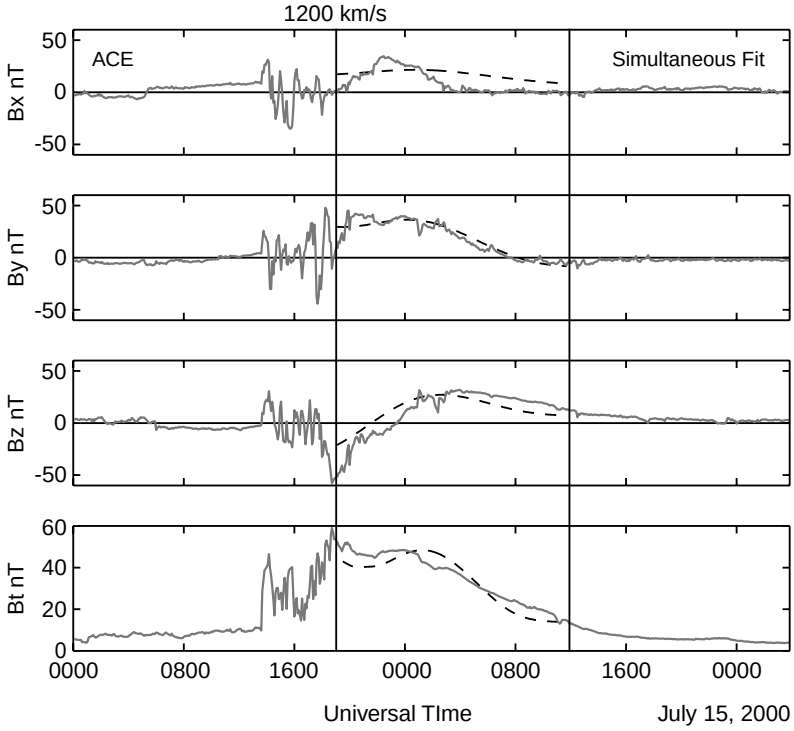

Fig. 2. ACE measurements in solar ecliptic coordinates of the interplanetary magnetic field through the so-called Bastille Day ICME at 1 AU courtesy of C.W. Smith.

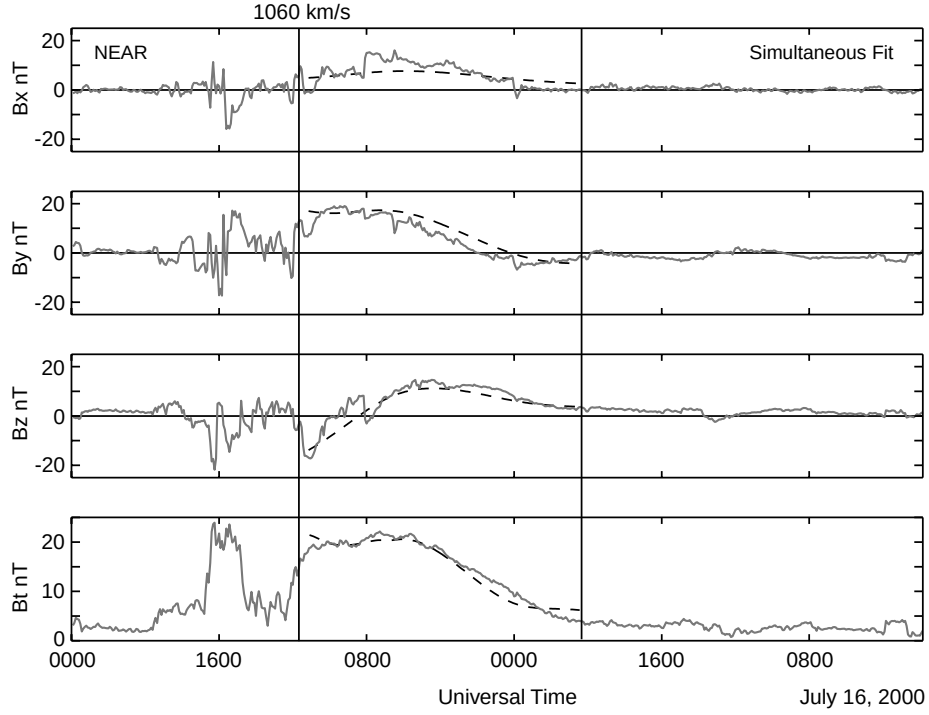

Fig. 3. NEAR measurements in Eros solar orbital coordinates of the interplanetary magnetic field through the Bastille Day ICME at 1.7 AU. This coordinate system has its X-axis to the sun and its XY plane is the orbital plane of Eros.

tion) and clock angles of 53° and 48° (where 0° is in the ecliptic plane). The magnetic flux contained in the ICME is a constant, 108 TWb. We do not have a solar wind velocity measurement at NEAR but we assume that the ICME does not decelerate. If so, the magnetosheath thickness has grown about a factor of two as the ICME moved to 1.7 AU.

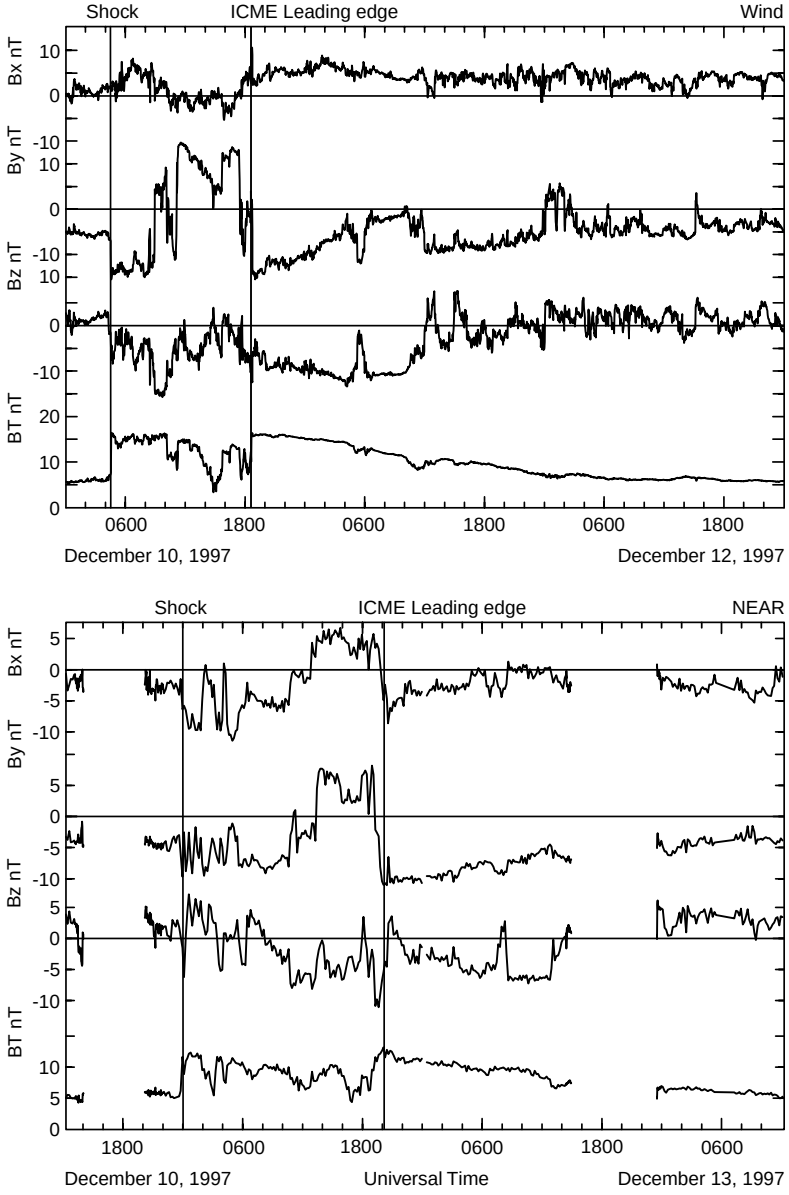

Fig. 4. (Top). Wind measurements in solar ecliptic coordinates of the interplanetary magnetic field at 1 AU during the December 10–11, 1997 ICME. (Bottom) NEAR measurements in NEAR solar orbital coordinates of the interplanetary magnetic field at 1.18 AU during the December 11–12 ICME.

A second example can be found in Fig. 4 measurements by Wind and NEAR at 1.0 and 1.18 AU on December 10–12, 1997 with an azimuthal separation of 1°. Here the shock grows from 0.13 to 0.18 AU in thickness, an increase of 38% as the ICME moves outward 18%.

At a single location data such as these are available over a full solar cycle at Pioneer Venus. Fig. 5 shows the thickness of these magnetosheaths normalized by the half thickness of the ICME. As mentioned in the introduction these thicknesses are quite large if we are to equate the ICME half thickness with the radius of curvature of the ICME obstacle. To aid in the interpretation of these data we next examine how to rewrite the formulas of Spreiter et al. (1966) and Farris and Russell (1994) in terms of the radius of curvature.

3. The effect of obstacle shape on shock location

Assuming that the obstacle can be represented by a simple conic section, we can express the distance from the focus of the conic section to the surface by

$$r = \frac{r_o(1+\varepsilon)}{1+\varepsilon\cos\theta}, \tag{1}$$

where ε is the eccentricity of the ellipse describing the shape of the boundary. We can then write the distance from the focus of the conic section to a point on the conic section in vector form.

$$\mathbf{r} = (1+\varepsilon)\left[\frac{\cos\theta}{1+\varepsilon\cos\theta}\,\hat{\mathbf{x}} + \frac{\sin\theta}{1+\varepsilon\cos\theta}\,\hat{\mathbf{y}}\right]. \tag{2}$$

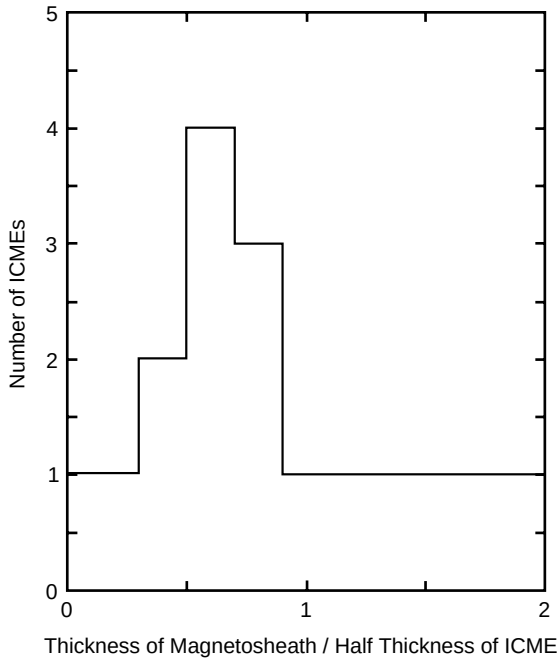

Fig. 5. Histogram of the thickness of ICME magnetosheaths normalized by the half-thickness of the ICMEs as seen at 0.72 AU by Pioneer Venus.

The radius of curvature, R_c, is defined as the reciprocal of the curvature

$$R_c = \sqrt{\frac{(\mathbf{r}' \bullet \mathbf{r}')^3}{(\mathbf{r}' \bullet \mathbf{r}')(\mathbf{r}'' \bullet \mathbf{r}'') - (\mathbf{r}' \bullet \mathbf{r}'')^2}}. \tag{3}$$

After some algebra we obtain

$$R_c = \frac{r_o(1+\varepsilon)}{1+\varepsilon\cos\theta}\sqrt{\frac{A(\varepsilon,\theta)}{B(\varepsilon,\theta)}}, \tag{4}$$

where A, B are algebraic functions of ε, θ.

For $\theta = 0$ (radius of curvature at the nose of the conic section), we find

$$\sqrt{\frac{A(\varepsilon,\theta)}{B(\varepsilon,\theta)}} = \sqrt{\frac{(1+\varepsilon)^6}{(1+\varepsilon)^4}} = 1+\varepsilon \tag{5}$$

and

$$R_c = \frac{r_o(1+\varepsilon)}{1+\varepsilon\cos\theta}\sqrt{\frac{A(\varepsilon,\theta)}{B(\varepsilon,\theta)}} = r_o(1+\varepsilon). \tag{6}$$

For the magnetopause, with $\varepsilon = 0.42$ for northward IMF and with focus at the center of the Earth, so $r_o = D_{OB}$, the radius of curvature (R_c) at the magnetopause nose ($10.3R_e$) is equal to the terminator distance $14.6R_e$.

The relation between the bow shock subsolar distance and the magnetopause can thus be written as (using the Spreiter et al., 1966 relation)

$$D_{BS} = D_{OB}\left[1 + 0.78\frac{R_c}{D_{OB}}\frac{\rho_\infty}{\rho_2}\right]. \tag{7}$$

This relation reduces to the laboratory result obtained for a spherical obstacle by Seiff (1962) ($\Delta/D_{OB} = 0.78\rho_\infty/\rho_2$) and gives the numerical result of Spreiter et al. (1966) ($\Delta/D_{OB} = 1.1\rho_\infty/\rho_2$) for a realistic magnetopause shape.

Spreiter et al. (1966) obtained the empirical formula

$$\frac{\Delta}{D_{OB}} = 1.1\,\frac{\rho_\infty}{\rho_2}, \tag{8}$$

where Δ is the distance from the obstacle boundary to the shock and D_{OB} are the distances from the center of the Earth to the top obstacle boundary. This formula is based on empirical data in the range $5 \leqslant M_s \leqslant 100$.

Landau and Lifshitz (1959) provide a formula of the density jump across the shock

$$\frac{\rho_\infty}{\rho_2} = \frac{(\gamma-1)M_\infty^2 + 2}{(\gamma+1)M_\infty^2}, \tag{9}$$

where M_∞ is the Mach number of the shock and γ is the adiabatic exponent.

Combining (8) and (9) gives

$$\frac{\Delta}{D_{OB}} = 1.1\,\frac{(\gamma-1)M_\infty^2 + 2}{(\gamma+1)M_\infty^2} \tag{10}$$

and rearranging

$$\frac{D_{BS}}{D_{OB}} = 1 + 1.1\,\frac{(\gamma-1)M_\infty^2 + 2}{(\gamma+1)M_\infty^2}. \tag{11}$$

This formula presents problems for low Mach number shocks because the shock location approaches a fixed distance from the obstacle as the Mach number approaches unity. In order to treat low Mach numbers Farris and Russell (1994) conjectured equation (8) could be rewritten

$$\frac{\Delta}{D_{OB}} = 1.1\,\frac{M_2^2}{1-M_2^2}. \tag{12}$$

In the asymptotic limit of $M_\infty \to \infty$, from Eq. (9) we obtain

$$\frac{\rho_\infty}{\rho_2} \to \frac{\gamma-1}{\gamma+1}.$$

Also it can be shown that the downstream Mach number has the asymptotic limit

$$M_2 \to \sqrt{\frac{\gamma-1}{2\gamma}}.$$

Thus

$$\frac{M_2^2}{1-M_2^2} \to \frac{\gamma-1}{\gamma+1}.$$

Landau and Lifshitz (1959) give the following formula for M_2:

$$M_2^2 = \frac{2 + (\gamma-1)M_\infty^2}{2\gamma M_\infty^2 - (\gamma-1)} \tag{13}$$

then, inserting (13) into (12)

$$\frac{D_{BS}}{D_{OB}} = 1 + 1.1\,\frac{(\gamma-1)M_\infty^2 + 2}{(\gamma+1)(M_\infty^2 - 1)}. \tag{14}$$

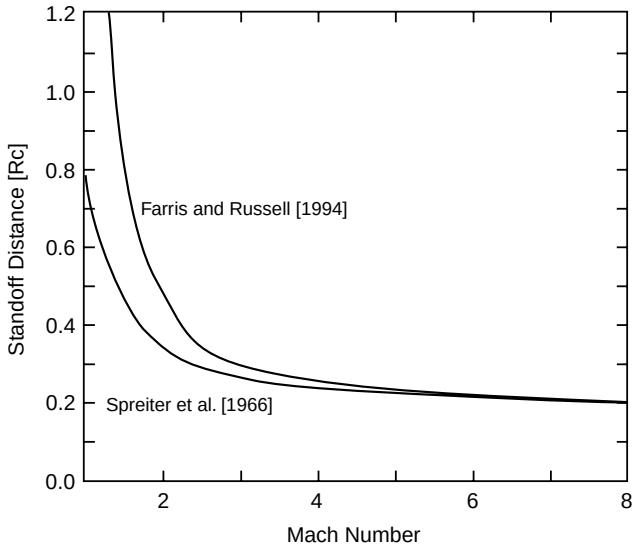

Fig. 6. Standoff distance of a shock from a spherical obstacle with radius of curvature, R_c, expressed in terms of the radius of curvature for the models of Spreiter et al. (1966) and of Farris and Russell (1994).

This formula has the attractive feature of moving the shock to infinity as the Mach number approaches unity as well as satisfying the high Mach number limit. We can rewrite this in terms of the radius of curvature, R_c, by noting that Spreiter et al's empirical constant of 1.1 was based on an obstacle with a nose radius of curvature of 1.35 given the ratio of its terminator distance to nose distance. Thus (14) may be rewritten:

$$\frac{\Delta}{R_c} = 0.81\,\frac{(\gamma-1)M_\infty^2+2}{(\gamma+1)(M_\infty^2-1)}. \tag{15}$$

For $\gamma = 5/3$ we can rewrite the separation distances from the shock to the obstacle for the Spreiter et al. (1966) approximation in terms of the radius of curvature

$$\Delta/R_c = 0.195 + 0.585M^{-2}. \tag{16}$$

While for the Farris and Russell (1994) approximation we obtain from (15)

$$\Delta/R_c = 0.195 + 0.78(M^2-1)^{-1}. \tag{17}$$

Substituting $M = 1$ in formula (16) we find that the Spreiter et al. (1966), approximation has a finite separation distance of $0.78R_c$ while from (17) the Farris and Russell (1994) approximation goes to infinity at $M = 1$.

These formulas are plotted versus the upstream Mach number in Fig. 6 for $\gamma = 5/3$ compared with the Spreiter et al. (1966) prediction, shown to low Mach numbers for which it was clearly stated in the original work that the formula was not appropriate.

4. What is the effective radius of curvature of an ICME?

A well-documented event for which we can examine this question is the nearly simultaneous observation of a rope by the International Sun-Earth Explorer (ISEE) and PVO on August 27 and 28, 1978 (Mulligan and Russell, 2001). For the ISEE 3/PVO event the Mach number was 3 and the standoff distance would be predicted to be 0.28 times the radius of curvature. Since the standoff distance was observed to be 0.11 AU, the radius of curvature must have been $R_c = 0.11/0.28 = 0.4$ AU.

This is inconsistent with a small cylindrical symmetric rope as the obstacle with a radius of 0.11 AU. Instead, the radius of curvature is determined partially by the axial bending that, if it resembles a dipolar field shape as shown in Fig. 1, is close to 0.4 AU. However, if the other characteristic radius of curvature were equal to the ICME half thickness, 0.11 AU, the effective radius of curvature would be 0.2 AU, the geometric mean of the two radii (Stahara et al., 1989). We must conclude that the radius of curvature is close to 0.4 AU in both directions orthogonal to the radius vector to the sun.

The August 27–28, 1978 event is a good example to use because the two observations at different azimuthal locations also allow an estimate of the longitudinal width of the obstacle and that width is about 0.8 AU (Mulligan and Russell, 2001). While the width of the structure is not strictly the same as the radius of curvature, the similarity of the values gives some assurance that a model of a thin curved obstacle with much greater width and height is the appropriate model. In other words the modification needed to the paradigm shown in Fig. 1 is to widen it about a factor of four into the plane of the page.

5. Discussion and conclusions

Multiple lines of evidence lead to the conclusion that ICMEs are not cylindrically symmetric. Above we have seen that the standoff distance of the shock is most consistent with an azimuthal extent that is about four times as wide as an ICME is thick. This is also consistent with the multipoint inversions of the ICMEs on August 27–28, 1978. Further, as discussed by Russell and Mulligan (2002), the impact parameter obtained in flux-rope fits, assuming cylindrical symmetry, are distributed in a manner inconsistent with the expected flat or random distribution that would result if the cylindrical assumption were true. Also shock normals appear to be more closely aligned in the radial direction than they would be if the front of the ICME were not blunter than in the standard ICME model.

This "modern" picture of the ICME and magnetic cloud is not greatly different from the pre-flux-rope paradigm. The magnetic clouds thought to be responsible for the modulation of galactic cosmic rays were large structures, not narrow ropes (Newkirk et al., 1981). Observations by Helios and Voyager (Burlaga et al., 1981) and Imager for Mars Pathfinder (IMP) 6–8 and Pioneer II (Crooker and Intriligator, 1996) also indicate a width of at least 30°. A similar conclusion was drawn by Crooker et al. (1990) based on the

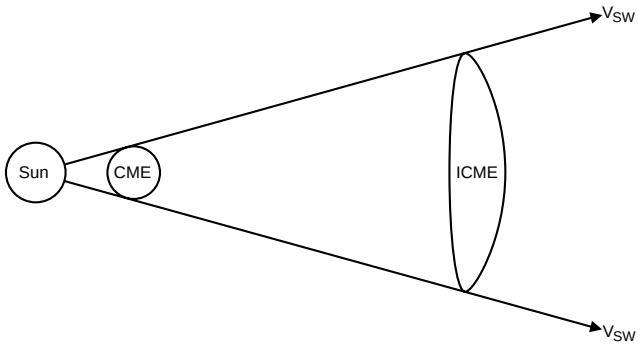

Fig. 7. Schematic of the radial and azimuthal expansion of an ICME in the plane perpendicular to the axis of the rope. Near the sun the CME has a circular cross section but the spreading of the solar wind flow lines stretches the ICME.

normals to discontinuities within an ICME structure. These normals were also aligned with the radius vector from the sun for the magnetic cloud to be rope like. The inferred structure was a large bubble rather than a tight cylindrical flux rope. In truth it appears that the ICME magnetic structure is an amalgam of the bubble and the flux-rope pictures. The field is twisted but the cross section seems not to be cylindrical in the neighborhood of 1 AU.

With the aid of Fig. 7 we can understand physically why the ICME might evolve into a flattened structure. If a cylindrical flux rope was created in the corona and carried outward, the magnetic stresses would attempt to keep it cylindrical in cross section. The solar wind plasma, on the other hand, would attempt to expand radially so that the structure kept a constant angular width. Thus once the solar wind forces were able to dominate over the magnetic forces the ICME should become azimuthally stretched. In fact such structures are produced in 3D magneto-hydrodynamics (MHD) simulations of the propagation of ICMEs (Odstrcil and Pizzo, 1999).

In short, there is much evidence now, both direct and indirect that points to the fact than ICMEs are not cylindrically symmetric. However, to properly invert a non-cylindrically symmetric structure requires multiple observations over a baseline that is a significant fraction of the scale size of the ICME. Until such time as multiple observations are more regularly available we will still need to use cylindrically symmetric models to fit these structures, but in doing so we should remember that the conclusions we can draw from such analyses are limited and the flux content of a rope might easily be a factor of four greater than the cylindrically symmetric value. Further we emphasize that these non-cylindrically symmetric structures are not force free. Thus it is easy to explain their expansion as typified by the Bastille Day Event shown in Figs. 2 and 3. The success of cylindrically symmetric force-free fits in replicating the structure revealed by single spacecraft observations is not indicative of the true nature of ICMEs.

Acknowledgements

This work was supported by the National Aeronautics and Space Administration under grant through the Johns Hopkins University, Applied Physics Laboratory and by a grant from the Los Alamos National Laboratory.

References

Burlaga, L.F., 1988. Magnetic clouds and force-free fields with constant alpha. J. Geophys. Res. 93, 7124–7217.

Burlaga, L.F., 2001. Ejecta in the solar wind. EOS Trans. AGU 82 (39), 434.

Burlaga, L.F., Sittler, E., Mariani, F., Schwenn, R., 1981. Magnetic loop behind an interplanetary shock: Voyager, Helios, and IMP 8 observations J. Geophys. Res. 86, 6673–6684.

Burlaga, L.F., Klein, L., Sheeley Jr., N.R., Michel, D.J., Koomen, R.A., Schwenn, R., Rosenbauer, H., 1982. A magnetic cloud and a coronal mass ejection. Geophys. Res. Lett. 9, 1317.

Burlaga, L.F., Lepping, R.P., Jones, J.A., 1990. Global configuration of a magnetic cloud. In: Russell, E.R., Priest, C.T., Lee, L.C. (Eds.), Physics of Magnetic Flux Ropes. AGU, Washington, DC, pp. 373–377.

Crooker, N.U., Intriligator, D.S., 1996. A magnetic cloud as a distended flux rope conclusion in the heliospheric current sheet. J. Geophys. Res. 101, 24,343–24,348.

Crooker, N.U., Gosling, J.T., Smith, E.J., Russell, C.T., 1990. A bubblelike coronal mass ejection flux rope in the solar wind. In: Russell, C.T., Priest, E.R., Lee, L.C. (Eds.), Physics of Magnetic Flux Ropes, Geophys. Mono, 58. AGU, Washington, DC, pp. 365–371.

Farris, M.H., Russell, C.T., 1994. Determining the standoff distance of the bow shock: Mach number dependence and use of models J. Geophys. Res. 99, 17,681–17,689.

Farrugia, C.J., Burlaga, L.F., Osherovich, V.A., Richardson, I.G., Freeman, M.P., Lepping, R.P., Lazarus, A.J., 1993a. A study of an interplanetary magnetic cloud and its interaction with the Earth's magnetosphere: the interplanetary aspect J. Geophys. Res. 98, 7621.

Farrugia, C.J., Richardson, I.G., Burlaga, L.F., Lepping, R.P., Osherovich, V.A., 1993b. Simultaneous observations of solar MeV particles in a magnetic cloud and in the Earth's northern tail lobe: implications for the global field line topology of magnetic clouds and for the entry of solar particles into the magnetosphere during cloud passage J. Geophys. Res. 98, 15,497–15,507.

Goldstein, H., 1983. On the field configuration of magnetic clouds. In: Neugebauer, M. (Ed.), Solar Wind Five, NASA Conf. Publ. 2280, Washington, DC, pp. 731–733.

Kahler, S.W., Reames, D.V., 1991. Probing the magnetic topologies of magnetic clouds by means of solar energetic particles. J. Geophys. Res. 96, 9419–9424.

Landau, L.D., Lifshitz, E.M., 1959. Fluid Mechanics. Addison-Wesley, Reading, MA, 536 pp.

Lepping, R.P., Jones, J.A., Burlaga, L.F., 1990. Magnetic field structure of interplanetary magnetic clouds at 1 AU. J. Geophys. Res. 95, 11,957–11,965.

Lindsay, G.M., Luhmann, J.G., Russell, C.T., Gosling, J.T., 1999. Relationships between coronal mass ejection speeds form coronagraph images and interplanetary characteristics of associated interplanetary coronal mass ejections. J. Geophys. Res. 104, 12,515–12,523.

Mulligan, T., Russell, C.T., 2001. Multi-spacecraft modeling of the flux rope structure of interplanetary coronal mass ejections: cylindrically symmetric versus non-symmetric topologies J. Geophys. Res. 106, 10,581–10,596.

Newkirk Jr., G., Hundhausen, A.J., Pizzo, V.J., 1981. Solar cycle modulation of galactic cosmic rays: speculation on the role of coronal transients J. Geophys. Res. 86, 5387–5396.

Odstrcil, D., Pizzo, V.J., 1999. Distortion of the interplanetary magnetic field by three-dimensional propagation of coronal mass ejections in a structured solar wind. J. Geophys. Res. 104, 28,225–28,239.

Richardson, I.G., Farrugia, C.J., Winterhalter, D., 1994. Solar activity and coronal mass ejections on the western hemisphere of the Sun in mid-August 1989: association with interplanetary observations at the ICE and IMP 8 spacecraft J. Geophys. Res. 99, 2513–2529.

Russell, C.T., 2001. In defense of the term ICME. EOS Trans. AGU 82 (39), 434.

Russell, C.T., Elphic, R.C., 1979. Observation of magnetic flux ropes in the Venus ionosphere. Nature 279, 616–618.

Russell, C.T., Mulligan, T., 2002. The true dimensions of interplanetary coronal mass ejections, Adv. Space Res., 29 (3), 301–306.

Schwenn, R., 1983. Direct correlation between coronal transient and interplanetary disturbances. Space Sci. Rev. 34, 85–99.

Seiff, A., 1962. Gasdynamics in space exploration. NASA Special Publication 24, Washington, DC, p. 19.

Sheeley, N.R., Howard, R.A., Koomen, M.J., Michels, D.J., Schwenn, R., Muhlhauser, K.H., Rosenbauer, H., 1985. Coronal mass ejections and interplanetary shocks. J. Geophys. Res. 90 (A1), 163–175.

Spreiter, J.R., Summers, A.L., Alksne, A.Y., 1966. Hydromagnetic flow around the magnetosphere. Planet. Space Sci. 14, 223–253.

Stahara, S.S., Rachiele, R.R., Spreiter, J.R., Slavin, J.A., 1989. A three dimensional gas dynamic model for the solar wind flow past nonaxisymmetric magnetospheres: application to Jupiter and Saturn J. Geophys. Res. 94, 13,353–13,365.